


 Cite this: *RSC Adv.*, 2026, **16**, 3021

Boosting the adsorption and sensing performance of MoS_2 for SF_6 decomposition gases by non-metal atom doping: a DFT study

Mamutjan Tursun, * Yifan Liu and Abulimiti Yumaier*

In electrical power systems, SF_6 in Gas Insulated Switchgear (GIS) decomposes under partial discharge, yielding toxic products such as H_2S , SO_2 , SOF_2 , SO_2F_2 . Molybdenum disulfide (MoS_2), a promising two-dimensional material, exhibits potential in gas sensing but its pristine form suffers from weak adsorption capacity for gas molecules. Herein, we carry out a systematic exploration of the gas-sensing capabilities of eight non-metal (NM)-doped MoS_2 (NM@ MoS_2) materials toward SF_6 decomposition gases by leveraging first-principles calculations. The results reveal that all NM@ MoS_2 substrates exhibit thermodynamic stability with negative binding energies ranging from -0.84 to -7.11 eV. Pristine MoS_2 shows weak physisorption of target gases, accompanied by low adsorption energies (-0.21 to -0.33 eV), large adsorption distances (2.90 to 3.70 Å), minimal charge transfer and limited sensitivity. In contrast, the NM@ MoS_2 substrates demonstrate distinct adsorption behaviors: O@ MoS_2 , Se@ MoS_2 , and Te@ MoS_2 retain physical adsorption (adsorption energies: -0.14 to -0.37 eV; distances: 2.73 to 4.02 Å), whereas B@ MoS_2 , C@ MoS_2 , N@ MoS_2 , P@ MoS_2 , and Si@ MoS_2 demonstrate enhanced adsorption (adsorption energies: -0.39 to -1.67 eV; distances: 1.60 to 3.24 Å), accompanied by significant charge transfer and enhanced sensing-response. Of these substrates, Si@ MoS_2 demonstrates moderate recovery times at ambient temperature (2.82 s) and demonstrates significant sensing-response to SF_6 decomposition components, highlighting its potential for practical gas sensing applications. This study demonstrates that non-metal doping can effectively enhance the gas-detection efficacy of MoS_2 towards SF_6 decomposition products, providing theoretical support for developing high-efficiency gas sensors.

 Received 5th November 2025
 Accepted 5th January 2026

DOI: 10.1039/d5ra08522e

rsc.li/rsc-advances

1. Introduction

In the realm of power systems, Gas Insulated Switchgear (GIS) has become increasingly prevalent as power grids expand, and its safe and reliable operation is of utmost importance.^{1,2} A key component of GIS is sulfur hexafluoride (SF_6), which serves as a vital gas-insulating medium, renowned for its remarkable electrical insulation and arc-quenching properties. However, during extended periods of operation, local discharge events can trigger the breakdown of SF_6 gas, producing byproducts such as hydrogen sulfide (H_2S), sulfur dioxide (SO_2), sulfonyl fluoride (SOF_2), and thionyl difluoride (SO_2F_2).^{3,4} These byproducts have significantly poorer insulating properties than SF_6 , which weakens equipment insulation, intensifies local discharge incidents and poses a severe threat to system stability.^{5,6} In light of these challenges, it is of the utmost importance to develop effective technologies that can detect and remove SF_6 decomposition gases. Such advancements are essential for enhancing the safety and reliability of power

systems, as well as for mitigating potential environmental and health risks.^{7,8}

In recent years, two-dimensional transition metal dichalcogenides (TMDs) have garnered significant attention due to their ultra-high specific surface area and exceptional electronic transport properties. Taking MoS_2 as an example, chemical vapor deposition (CVD) enables the fabrication of atomic-thickness monolayer films.⁹ When thickness is reduced to the atomic level, the specific surface area increases significantly, expanding the interface area for gas molecule contact. Simultaneously, the bandgap transitions from the bulk indirect bandgap (1.2 eV) to a direct bandgap (1.8 eV), substantially enhancing electron mobility and accelerating rapid charge transfer between gas molecules and the surface.¹⁰ These attributes have propelled their extensive utilization in gas sensing applications.¹¹⁻¹⁴ Additionally, atomically functionalized TMDs have been employed for detecting SF_6 decomposition gases. For instance, Li *et al.* demonstrated the potential of platinum-doped HfS_2 (Pt-HfS_2) for dual gas detection of H_2S and SO_2 .¹⁵ Jiang *et al.* investigated the adsorption behavior of iridium-embedded hafnium disulfide (Ir-HfS_2) monolayers toward three sulfur hexafluoride decomposition products (H_2S , SOF_2 , and SO_2F_2) and their sensing prospects.¹⁶ TMDs are

Xinjiang Key Laboratory of Novel Functional Materials Chemistry, College of Chemistry and Environmental Sciences, Kashi University, Kashi 844000, PR China.
 E-mail: mmtj15@stu.xjtu.edu.cn



characterized by a layered two-dimensional structure, where each layer is composed of alternating transition metal and chalcogen atoms. This unique structural arrangement imparts distinctive properties to TMDs, unlocking a wide range of potential applications.^{17,18} Currently, extensive research efforts have been directed toward exploring two-dimensional materials, particularly compounds such as MoS₂, MoSe₂, and SnS₂.¹⁹⁻²² Investigations have revealed that TMDs monolayer exhibits favorable characteristics, including narrow band gaps and high carrier mobility. These features render them highly suitable for applications in optoelectronics and nanoelectronics.²³⁻²⁵

Among TMDs materials, MoS₂ has attracted the most research interest in gas detection, particularly for the sensing of toxic gases. This is due to its favourable semiconductor properties, which include a substantial band gap, a large surface-to-volume ratio, an abundance of sites for redox reactions, and high carrier mobility.^{26,27} MoS₂-based gas sensing materials achieve significant gas sensitivity through charge transfer between gas molecules and the surface. For instance, Late *et al.* utilised *ab initio* calculations to ascertain that the observed reduction in resistance of monolayer and bilayer MoS₂ under an applied magnetic field is attributable to charge transfer.²⁸ Dong *et al.* fabricated an Au/MoS₂/Au photoelectrochemical gas sensor exhibiting sensitivity as high as $S = 4.9\%/\text{ppb}$ (49000/ ppm) upon exposure to ppb-level NO₂.²⁹ However, chemical adsorption impedes recovery processes, and MoS₂ still faces bottlenecks such as poor selectivity and insufficient sensitivity.³⁰ Therefore, new strategies are urgently needed to overcome performance limitations.

In recent decades, a vast body of research has concentrated on modifying the MoS₂ monolayer to improve its gas-sensing performance. These modification strategies primarily include doping with metal (both precious and non-precious metals) and non-metal (NM) atoms, as well as compositing with other materials.^{27,31-39} Such modifications are credited with significantly improving the electronic properties and structural stability of MoS₂ monolayers, thereby optimizing their gas-sensing capabilities.^{31,39} Therefore, doping has a significant influence on the electronic structure and gas-detection capability of MoS₂, including the adsorption strength, interfacial charge displacement and adsorbate–substrate interaction. For example, Fan *et al.* studied how the doping of transition metals (including several precious and non-precious metals) affects the gas-detecting performance of MoS₂ monolayer when exposed to various gas molecules (CO, NO, O₂, NO₂ and NH₃).³⁷ The results demonstrated that doping significantly enhanced the sensing performance. Luo *et al.* selected Al, Si, and P atoms as dopants due to the close similarity of their covalent radii to that of the S atom.³⁸ Doping MoS₂ with these atoms has demonstrated promising potential for NO₂ sensing despite of hazardous gasses sensing, the MoS₂ doped with metal (both precious and non-precious metals) atom materials also used detection of SF₆ decomposition gases.^{3,36,40,41}

Similarly, extensive research has been conducted on utilizing NM atoms to modify MoS₂ for detecting sulfur-containing gases.^{42,43} For instance, Szary *et al.* systematically investigated

adsorption selectivity by adsorbing H₂S, N₂, and O₂ molecules on pristine MoS₂ films and MoS₂ films doped with P, Cl and Ge.⁴² Piosik *et al.* used doping strategies involving Si, P, Cl, Ge and Se to significantly improve the sensing performance of MoS₂ for SO₂.⁴³ It should be emphasized that MoS₂ substrates doped with NM atoms are renowned for the simplicity of their preparation. For instance, through density functional theory (DFT) calculations, Ma and his colleagues showed that common gases such CO, NO, NO₂, and O₂ are capable of occupying S vacancies in MoS₂ at room temperature. In this way, doping with C, N, and O can be realized.⁴⁴ This implies that MoS₂ doped with NM atoms can be realized under gentle conditions. Moreover, Song and his colleagues managed to synthesize P-doped MoS₂ through a simple pyrolysis procedure.⁴⁵ Xie and their team successfully fabricated MoS₂ materials with different concentrations of oxygen doping by controlling the preparation temperature.⁴⁶ Zhang and his colleagues fabricated Se-doped MoS₂ materials employing a hydrothermal process, and Song *et al.* produced O-doped MoS₂ materials by means of pyrolysis.^{47,48} In a similar vein, multiple experimental studies have emphasized that B-doped MoS₂ materials obtained *via* the hydrothermal route display outstanding performance in electrocatalytic reactions.⁴⁹⁻⁵¹ Consequently, these research outcomes provide strong theoretical backing for the synthesizability and stability of NM@MoS₂ materials.

In this study, we performed a comprehensive analysis of the adsorption and detection characteristics of NM@MoS₂ materials (where NM = B, C, N, O, P, Si, Se and Te) using DFT calculations, with regard to four SF₆ decomposition products: H₂S, SO₂, SOF₂ and SO₂F₂. Firstly, we calculated the formation energies of NM@MoS₂ to evaluate the thermodynamic stability of the different substitution sites. Next, we computed and analyzed the adsorption characteristics of the four SF₆ decomposition gases on NM@MoS₂ substrates, making comparisons with intrinsic MoS₂. Finally, we explored their gas-sensing potential further *via* electronic structure calculations and sensitivity analysis.

2. Computational methods

We performed spin-polarized DFT calculations using the Vienna *Ab Initio* Simulation Package (VASP).⁵² The electronic exchange and correlation terms were characterised using the generalized gradient approximation (GGA) and the Perdew–Burke–Ernzerhof (PBE) functional.⁵³ The GGA-PBE functional is one of the most widely used exchange-correlation approximations for evaluating electronic properties. Compared to the Local Density Approximation (LDA), *meta*-GGA, and hybrid functions, it strikes a favourable balance between computational cost and accuracy, and it has also been extensively studied for calculations involving two-dimensional materials.^{3,41,44} Ion–electron interactions were characterized using the Projector Augmented Wave (PAW) approach, and the energy cutoff was fixed at 450 eV.⁵⁴ Complete relaxation was achieved for every atom, with standard convergence parameters of 1×10^{-4} eV and 0.02 eV \AA^{-1} established for energies and forces, respectively. The DFT-D3 approach was then employed to



strengthen the weak van der Waals forces between the adsorbates and surfaces.⁵⁵ The limited capability of traditional functions in describing dispersion effects makes the introduction of empirical dispersion correction terms the most viable solution currently available.⁵⁶ Compared to methods such as DFT-D2 and optPBE, the DFT-D3 correction technique offers greater accuracy, broader elemental coverage (H–Pu) and improved computational efficiency.⁵⁷ It is particularly well-suited to large-scale or rapidly iterative research systems, and has been widely adopted in chemistry, materials science and related fields.^{58,59} During the geometry optimization process, a $4 \times 4 \times 1$ Monkhorst–Pack k -point grid was adopted to sample the Brillouin zone.⁶⁰ A single-layer supercell with dimensions of $4 \times 4 \times 1$ was built to serve as a model for the substrate surface. To eradicate the possible effect of periodicity on computational results, a 15 Å-thick vacuum layer was established in the lattice's Z -direction. To examine the possibility of doping MoS_2 with NM atom, the formation energies (E_f) of NM@ MoS_2 substrates were computed in line with eqn (1):

$$E_f = E_{\text{NM@MoS}_2} - E_{\text{MoS}_2} - \mu_{\text{NM}} + \mu_{\text{substitute-atom}} \quad (1)$$

where, E_{MoS_2} and $E_{\text{NM@MoS}_2}$ represent the total energy of a single-layer $4 \times 4 \times 1$ MoS_2 supercell, and the total energy of the system after one S or Mo atom in the supercell is substituted with an NM atom, respectively. μ_{NM} represents the chemical potential of the NM atom. With regard to N and O atoms, their respective values are derived from the per-atom energies of their gaseous forms (N_2 and O_2). For all other types of atoms, their chemical potentials are obtained from the per-atom energies of their bulk or solid states: specifically, β -rhombohedral boron for B, graphite for C, black phosphorus for P, diamond-cubic silicon for Si, trigonal selenium for Se, hexagonal tellurium for Te. $\mu_{\text{substitute-atom}}$ represents the chemical potential of the replacement atom. NM atoms can replace either the S sites or Mo sites in MoS_2 . The chemical potentials of S and Mo correspond to the energy per atom in the 8-membered rings and body-centered cubic (bcc) structures.

The adsorption energies (E_{ad}) of adsorbed gases are calculated according to eqn (2):

$$E_{\text{ad}} = E_{\text{NM@MoS}_2+\text{adsorbed gas}} - E_{\text{NM@MoS}_2} - E_{\text{gas molecule}} \quad (2)$$

where, $E_{\text{NM@MoS}_2+\text{adsorbed gas}}$ is the total energy of NM@ MoS_2 adsorption system, $E_{\text{NM@MoS}_2}$ is the energy of NM@ MoS_2 substrate, and $E_{\text{gas molecule}}$ is the energy of an isolated gas molecule. All these energies were computed from optimized atomic structures.

3. Results and discussion

3.1. Structural stability of NM@ MoS_2

Starting from the 2H- MoS_2 unit cell, the geometric structure was first optimized to obtain lattice parameters. The optimized lattice constant was $a = 3.16$ Å, the S–Mo bond length was 2.41 Å, and the S–Mo–S bond angle was 80.61°, which are highly consistent with literature reports.^{61,62} Given that MoS_2

monolayer features two substitutional sites (*i.e.*, S and Mo), this study systematically investigated the substitution of B, C, N, O, P, Si, Se, and Te at both sites. The corresponding configurations are presented in Fig. 1a and S1a. To quantitatively evaluate the synthetic feasibility of these NM@ MoS_2 materials, we initially computed their formation energies (E_f). As illustrated in Fig. 1b and S1b, the E_f values of NM atoms substituting S sites in MoS_2 monolayer range from –3.86 to 2.32 eV, whereas those substituting Mo sites span from –0.22 to 9.52 eV. The substantially lower energy barrier for S-site substitution highlights a distinct preference of NM atoms for occupying the S positions. It is noteworthy that although the E_f value for N atom replacing the S site is relatively large, this result stems from setting the chemical potential of the N atom to half that of nitrogen gas in this work. Nevertheless, the E_f value for N atom replacing S site remains significantly lower than the corresponding value for replacing the Mo site, indicating that the N atom preferentially substitutes the S site. Experimental synthesis of N@ MoS_2 via S-site substitution has already been achieved,^{63,64} thereby confirming its experimental feasibility and stability. Besides, the majority of other NM@ MoS_2 materials have been successfully synthesized experimentally, which further validating their stability.^{44–48,51} Huang *et al.* successfully synthesized ultrathin P-doped MoS_2 nanosheets *via* pyrolysis, achieving a surface phosphorus content of 4.7 at%.⁴⁵ Xie *et al.* used hydrothermal synthesis to produce oxygen-doped MoS_2 ultrathin nanosheets (O- MoS_2), with oxygen atom content ranging from 1.92 to 4.18 at%.⁴⁶ Huang *et al.* thermally decomposed MoS_2 ultrathin nanosheets synthesized using ammonium molybdate, thiourea, and layered g-C₃N₄ as templates. Following simple H_2O_2 treatment, they achieved controlled oxygen atom introduction at defect sites (including edges), yielding an oxygen content of 6.2 at%.⁴⁷ Yuan *et al.* synthesized N-doped MoS_2 photocatalysts *via* a two-step hydrothermal calcination process, achieving a nitrogen content of approximately 18.39 at%.⁶⁵

On the basis of the analysis mentioned above, we have gone for the S-site substitution of NM@ MoS_2 .

3.2. Adsorption performance analysis

3.2.1. Adsorption on pristine MoS_2 . The adsorption characteristics of four SF₆ decomposed gases on the pristine MoS_2 structure were comprehensively examined. The optimized configurations of H₂S, SO₂, SOF₂, and SO₂F₂ on pristine MoS_2 are shown in Fig. 2, and the corresponding adsorption energy (E_{ad}), adsorption distance (d), as well as the transferred charges (Q), are summarized in Table 1.

Since adsorption configurations vary with surface structure, " d " must be explicitly defined for each system. In the case of SO₂F₂ bonding to the sulfur site on the pristine MoS_2 surface *via* its sulfur atom, and the corresponding d is defined as the nearest interatomic distance from the SO₂F₂–S bond to the surface S atom. In NM@ MoS_2 system, SO₂F₂ couples to the NM site *via* oxygen atom. Here d is defined as the shortest distance from SO₂F₂–O bond to the NM atom. H₂S adsorbs onto the surface chalcogen site *via* the hydrogen atom, with d being



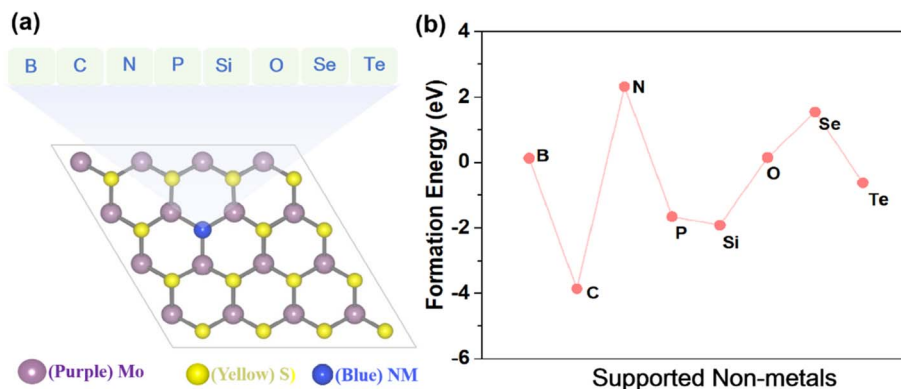


Fig. 1 (a) Structure of NM atoms replacing S sites in a monolayer MoS₂; (b) formation energies of NM atom substitutions at S sites in a monolayer MoS₂.

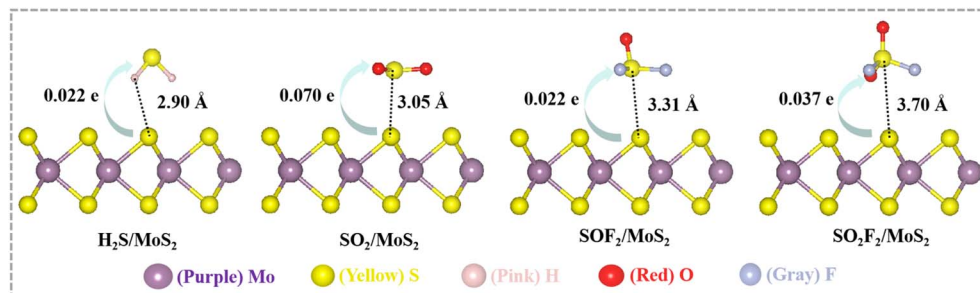


Fig. 2 Optimized structure of adsorbed gases on pristine MoS₂. Green directional lines show the number of transferred charges, and dashed lines represent the adsorption distance.

defined as the distance from H₂S–H to the corresponding chalcogen atom. SO₂ and SOF₂ both adsorb onto the surface sulfur site or dopant site *via* the sulfur atom, with *d* defined as the shortest distance from adsorbate–S to the sulfur or NM atom.

Based on Fig. 2 and Table 1, the adsorption efficiency of pristine MoS₂ towards the four gases is comparatively low ($E_{ad} \approx -0.30$ eV), with the corresponding *d*-values range from 2.9 to 3.7 Å, suggesting that the adsorption process is of a physisorptive in nature. In this scenario, charges consistently transfer from the MoS₂ substrate to the gas molecules, with corresponding *Q* values of merely 0.022, 0.070, 0.022, and 0.037 e. van der Waals forces are weak intermolecular interactions originating from transient charge fluctuations, with strengths significantly lower than those of covalent or ionic bonds.⁶⁶ Following adsorption onto the pristine MoS₂ surface, the *d* values of the four gases are significantly greater than the sum of the S–S covalent radii. Consequently, no chemical bonds are formed or broken. The interaction between these four gas

molecules and the pristine MoS₂ surface is primarily dominated by van der Waals forces. Given the relatively low E_{ad} , greater adsorption distances, and smaller quantities of charge transfer, it can be inferred that pristine MoS₂ exhibits limited adsorption capability toward H₂S, SO₂, SOF₂, and SO₂F₂.

3.2.2 Adsorption on NM@MoS₂. Fig. 3 and 4 show the optimized configurations of H₂S, SO₂, SOF₂ and SO₂F₂ on NM@MoS₂, with the corresponding *d* and *Q* values labelled on the respective configurations. The E_{ad} of these four gases on NM@MoS₂ are summarized in Tables 2 and 3.

This study categorises dopant atoms as either chalcogens (O, Se and Te) or non-chalcogens (B, C, N, P and Si). Non-chalcogen doping significantly enhances the gas adsorption capacity, as evidenced by the E_{ad} values of the four gases adsorbed on the NM@MoS₂ substrate. As shown in Table 2, the E_{ad} values of O@MoS₂, Se@MoS₂, and Te@MoS₂ exhibit range from -0.14 to -0.37 eV, indicating a lack of significant adsorption enhancement compared to pristine MoS₂ (-0.21 to -0.33 eV).

As shown in Table 3, the E_{ad} values of B@MoS₂, C@MoS₂, P@MoS₂, N@MoS₂ and Si@MoS₂ range from -0.39 to -1.67 eV, indicating enhanced adsorption. This adsorption enhancement is reflected by the significant reduction in the intermolecular distance between the substrate and the molecules. It can be concluded that a shorter adsorption distance generally implies a closer interaction between the gas molecule and the NM@MoS₂ substrate. The relatively short distance of adsorption implies a more intimate contact, aligns with its higher

Table 1 E_{ad} , *d*, and *Q* of adsorbed gases on pristine MoS₂

Adsorbed gases	E_{ad} (eV)	<i>d</i> (Å)	<i>Q</i> (e)
H ₂ S	-0.21	2.90	0.022
SO ₂	-0.33	3.05	0.070
SOF ₂	-0.29	3.31	0.022
SO ₂ F ₂	-0.33	3.70	0.037



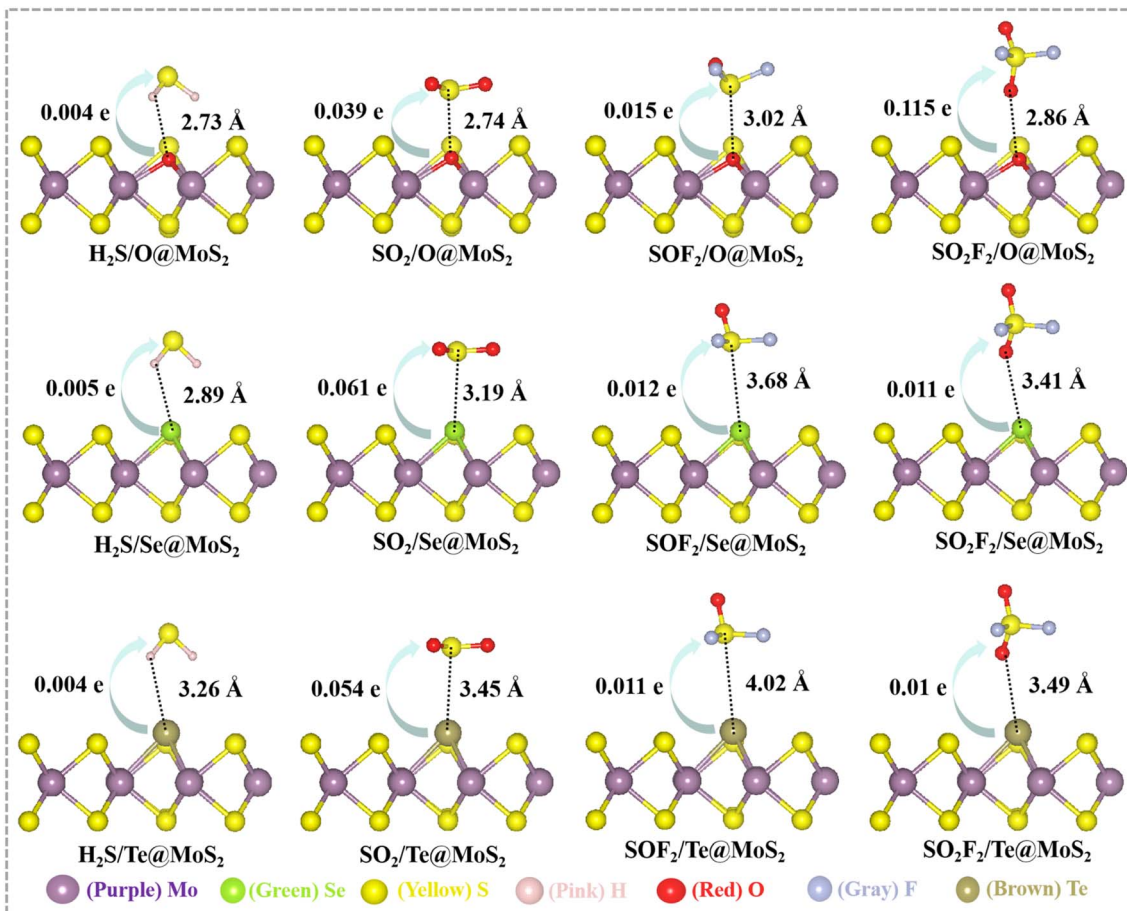


Fig. 3 Optimized structure of adsorbed gases on $\text{O}@\text{MoS}_2$, $\text{Se}@\text{MoS}_2$ and $\text{Te}@\text{MoS}_2$, respectively. Green directional lines show the number of transferred charges, and dashed lines represent the adsorption distance.

adsorption energy. In contrast, the longer distance of adsorption may be related to its relatively weaker interaction with $\text{NM}@\text{MoS}_2$ substrate. In terms of the transferred charge (Q), the amount of charge transfer reflects the degree of electron interaction during adsorption. The adsorption process shows a significant charge transfer, indicating a strong electron - donating or - accepting behaviour in the adsorption process, which associated with its relatively high adsorption energy as well.

We systematically compared the calculated adsorption energies with those of previously reported doping strategies (see Table S1), which further confirms the significant application potential of single-layer $\text{NM}@\text{MoS}_2$ (where $\text{NM} = \text{B, C, N, P or Si}$) in gas sensing. The study also reveals that MoS_2 substituted with transition metal atoms has a significantly higher adsorption capacity for SF_6 decomposition components.^{3,40,67,68} However, the excessively strong adsorption strength makes the adsorption sites difficult to regenerate, which severely hinders sensor recovery. In contrast, H_2S , SO_2 , SOF_2 , and SO_2F_2 exhibit insufficient adsorption stability on the PtSe_2 surface and readily desorbing at room temperature due to thermal agitation.⁶⁹ Compared to these materials, SF_6 decomposition gases show moderately reduced adsorption strength on the $\text{NM}@\text{MoS}_2$

monolayer, thereby avoiding the regeneration hindrance caused by excessively strong chemisorption.^{15,16,70-72}

In summary, the adsorption of SF_6 decomposition gases onto eight $\text{NM}@\text{MoS}_2$ substrates can be categorized into two group: substitution systems involving chalcogen elements (O, Se, Te) retain the original surface characteristics of MoS_2 and have no significant impact on the adsorption behavior of SF_6 decomposition products. In contrast, substitution systems involving non-chalcogen elements (B, C, N, P and Si) exhibit distinct adsorption properties, indicating that surface modification significantly alters gas adsorption behaviour.

3.2.3 Analysis of electronic properties. In view of the preceding analysis of the adsorption of H_2S , SO_2 , SOF_2 and SO_2F_2 gases onto $\text{B}@\text{MoS}_2$, $\text{C}@\text{MoS}_2$, $\text{N}@\text{MoS}_2$, $\text{P}@\text{MoS}_2$ and $\text{Si}@\text{MoS}_2$ substrates, which was classified as chemical adsorption, we further investigated the interaction mechanism between dopant atoms and adsorbed molecules by calculating the partial density of states (PDOS). As presented in Fig. 5, significant orbital hybridization occurs between the dopant (B, C, N, P and Si) atoms and the atoms of the adsorbed molecules. Fig. 5, for example, shows that the B-2p orbital in $\text{B}@\text{MoS}_2$ overlaps substantially with the S-3p, O-2p, and F-2p orbitals of the adsorbed gases. The same phenomenon also occurs for the $\text{C}@\text{MoS}_2$, $\text{N}@\text{MoS}_2$, $\text{P}@\text{MoS}_2$ and $\text{Si}@\text{MoS}_2$ substrates

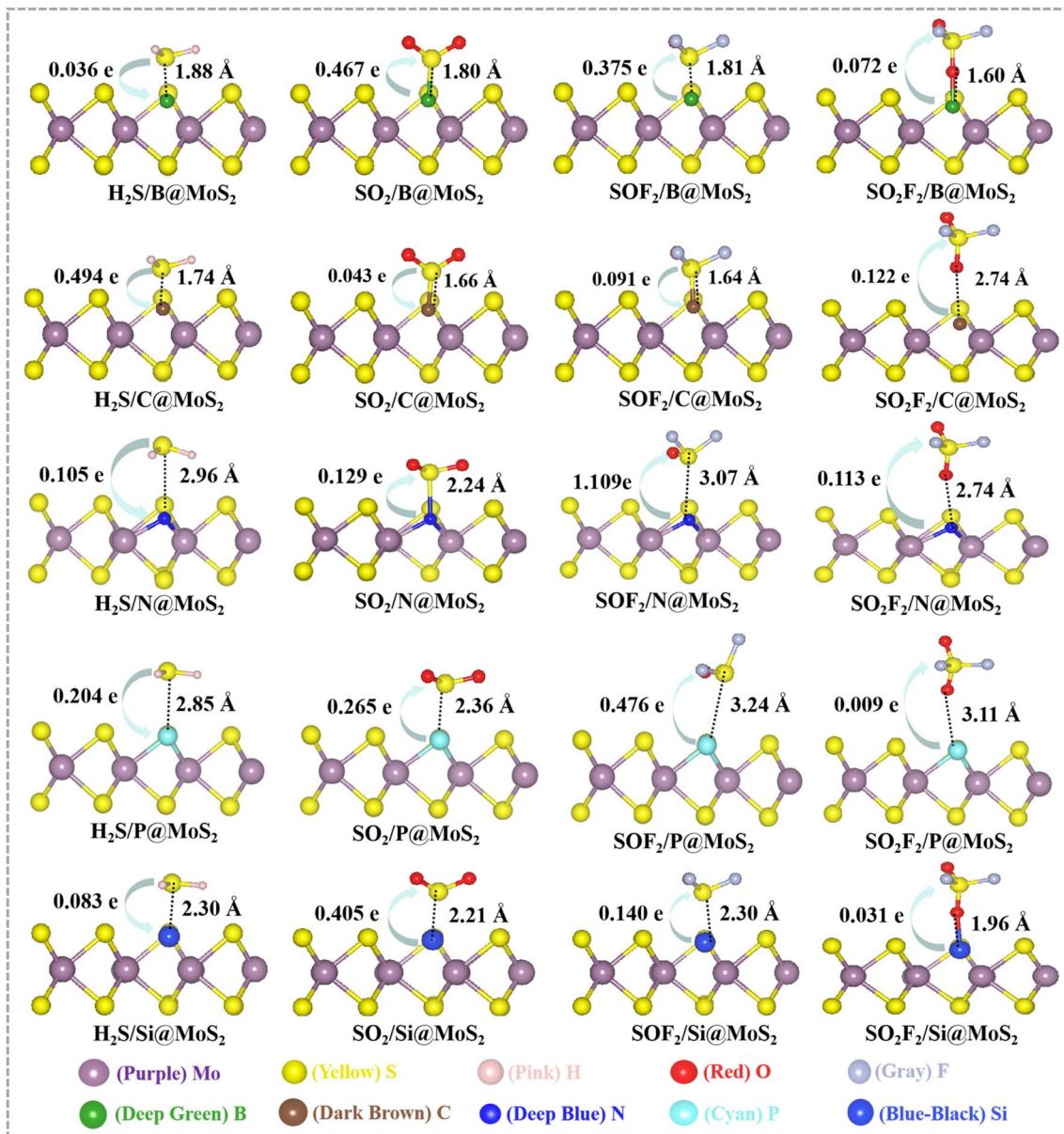


Fig. 4 Optimized structure of adsorbed gases on B@MoS₂, C@MoS₂, N@MoS₂, P@MoS₂, and Si@MoS₂, respectively. Green directional lines show the number of transferred charges, and dashed lines represent the adsorption distance.

(see Fig. 5). These results indicate that the obvious orbital hybridization between the dopant atoms (B, C, N, P and Si) and the atoms of the adsorbed molecules further explains the strong E_{ad} and short d between the adsorbed molecules and the substrates.

Table 2 E_{ad} of adsorbed gases on NM@MoS₂ (NM = O, Se, Te)

Substrates	E_{ad} (eV)			
	H ₂ S	SO ₂	SOF ₂	SO ₂ F ₂
O@MoS ₂	-0.32	-0.37	-0.33	-0.31
Se@MoS ₂	-0.15	-0.26	-0.23	-0.26
Te@MoS ₂	-0.14	-0.20	-0.19	-0.24

3.3. Recovery time

A high-performance gas sensor demands strong sensitivity toward the sensing gas, as well as a moderate recovery (desorption) time after adsorption. As previously confirmed,

Table 3 E_{ad} of adsorbed gases on NM@MoS₂ (NM = B, C, N, P, Si)

Substrates	E_{ad} (eV)			
	H ₂ S	SO ₂	SOF ₂	SO ₂ F ₂
B@MoS ₂	-1.66	-1.22	-0.98	-0.49
C@MoS ₂	-1.62	-1.15	-1.00	-0.44
N@MoS ₂	-0.46	-0.68	-0.51	-0.39
P@MoS ₂	-0.55	-0.75	-0.44	-0.39
Si@MoS ₂	-1.67	-0.93	-0.64	-0.74

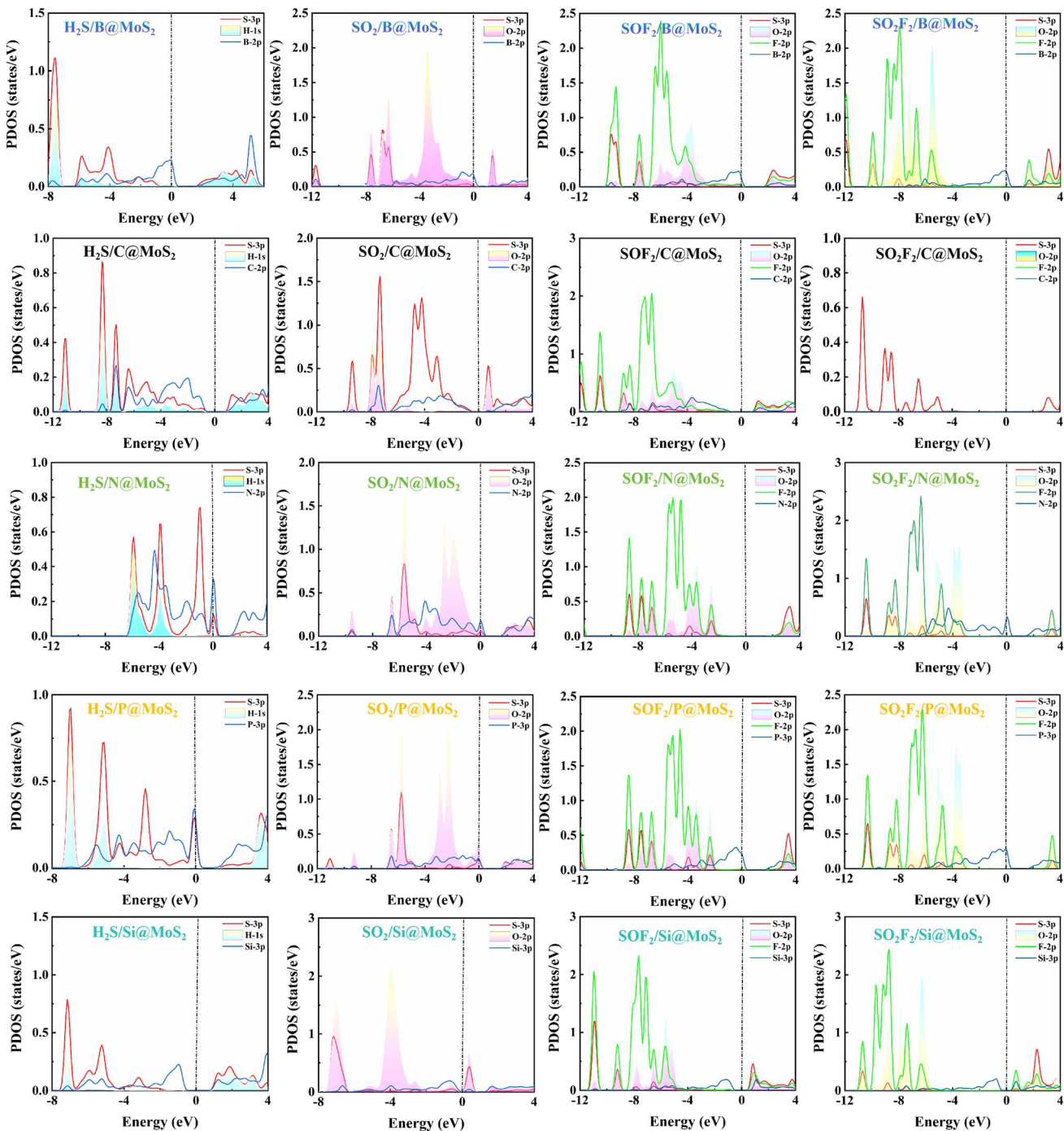


Fig. 5 PDOS of H_2S , SO_2 , SOF_2 and SO_2F_2 adsorbed on B@MoS_2 , C@MoS_2 , N@MoS_2 , P@MoS_2 and Si@MoS_2 substrates, respectively.

B@MoS_2 , C@MoS_2 , N@MoS_2 , P@MoS_2 and Si@MoS_2 substrates exhibit excellent adsorption efficiency for H_2S , SO_2 , SOF_2 and SO_2F_2 molecules. This section examines the scientific feasibility of using these materials in practice by exploring the specifics of recovery time during the desorption process. Recovery time is can be calculated using eqn (3):⁴

$$\tau = \frac{\exp\left(\frac{-E_{\text{ad}}}{K_B T}\right)}{\omega} \quad (3)$$

where, the experimental frequency (ω) corresponds to the vibration frequency of surface atoms and is set to 10^{12} s^{-1} .⁷³⁻⁷⁵ T is temperature (K), and K_B is the Boltzmann constant, which has a value of $8.62 \times 10^{-5} \text{ eV K}^{-1}$.

A moderate recovery period is essential for gas-sensing materials and is correlated with adsorption strength.^{4,6} Stronger adsorption of gases enhances the influence of individual molecule–substrate interactions, leading to a prompt and clear response. However, excessively strong adsorption can also slow down the recovery process. Therefore, the optimal

Table 4 Recovery times (in s) at 298 K, 398 K, and 498 K

System	Gas	298 K	398 K	498 K
B@MoS ₂	H ₂ S	1.27×10^{16}	1.11×10^9	6.85×10^4
	SO ₂	4.04×10^8	2.68×10^3	2.14
	SOF ₂	3.11×10^4	2.23	7.40×10^{-3}
	SO ₂ F ₂	1.97×10^{-4}	1.62×10^{-6}	9.18×10^{-8}
C@MoS ₂	H ₂ S	2.99×10^{15}	3.73×10^8	2.79×10^4
	SO ₂	3.56×10^7	4.35×10^2	5.0×10^{-1}
	SOF ₂	9.45×10^4	5.13	1.44×10^{-2}
	SO ₂ F ₂	3.38×10^{-5}	4.33×10^{-7}	3.20×10^{-8}
N@MoS ₂	H ₂ S	6.61×10^{-5}	7.17×10^{-7}	4.78×10^{-8}
	SO ₂	3.28×10^{-1}	4.18×10^{-4}	7.78×10^{-6}
	SOF ₂	5.50×10^{-4}	3.50×10^{-6}	1.70×10^{-7}
	SO ₂ F ₂	4.22×10^{-6}	9.13×10^{-8}	9.21×10^{-9}
P@MoS ₂	H ₂ S	1.73×10^{-3}	8.27×10^{-6}	3.38×10^{-7}
	SO ₂	3.39	3.41×10^{-3}	4.15×10^{-5}
	SOF ₂	2.67×10^{-5}	3.64×10^{-7}	2.78×10^{-8}
	SO ₂ F ₂	1.03×10^{-6}	3.19×10^{-8}	3.79×10^{-9}
Si@MoS ₂	H ₂ S	1.73×10^{16}	1.39×10^9	4.51×10^4
	SO ₂	5.62×10^3	5.92×10^{-1}	2.55×10^{-3}
	SOF ₂	6.11×10^{-2}	1.19×10^{-4}	2.84×10^{-6}
	SO ₂ F ₂	2.82	2.10×10^{-3}	2.81×10^{-5}

adsorption strength must strike a balance between recovery behaviour and response capability. Intrinsic MoS₂ exhibits weak adsorption for SF₆ decomposition gas, resulting in an extremely short recovery time and limited response capability. However, doping with non-halogen elements (B, C, N, P and Si) enhances adsorption strength to a moderate level, thereby optimizing the recovery time. Recovery times of H₂S, SO₂, SOF₂ and SO₂F₂ gases at 298 K, 398 K and 498 K were summarized in Table 4.

As shown in Table 4, a rise in temperature leads to an enhancement in the intensity of molecular Brownian motion, thereby shortening the recovery time. Therefore, controlling temperature is an effective way to adjust the system's recovery time. However, the B@MoS₂ and C@MoS₂ substrates have prolonged recovery times because they have high adsorption energies for H₂S, SO₂ and SOF₂ molecules. Meanwhile, the Si@MoS₂ substrate exhibits a prolonged recovery time for H₂S and SO₂ molecules at room temperature. Even at an elevated temperature of 498 K, the recovery times for the H₂S/B@MoS₂, H₂S/C@MoS₂ and H₂S/Si@MoS₂ systems are still extremely long at 6.85×10^4 s, 2.79×10^4 s and 4.51×10^4 s, respectively. Therefore, for systems with high adsorption energies, integrating with heating or UV irradiation is essential for

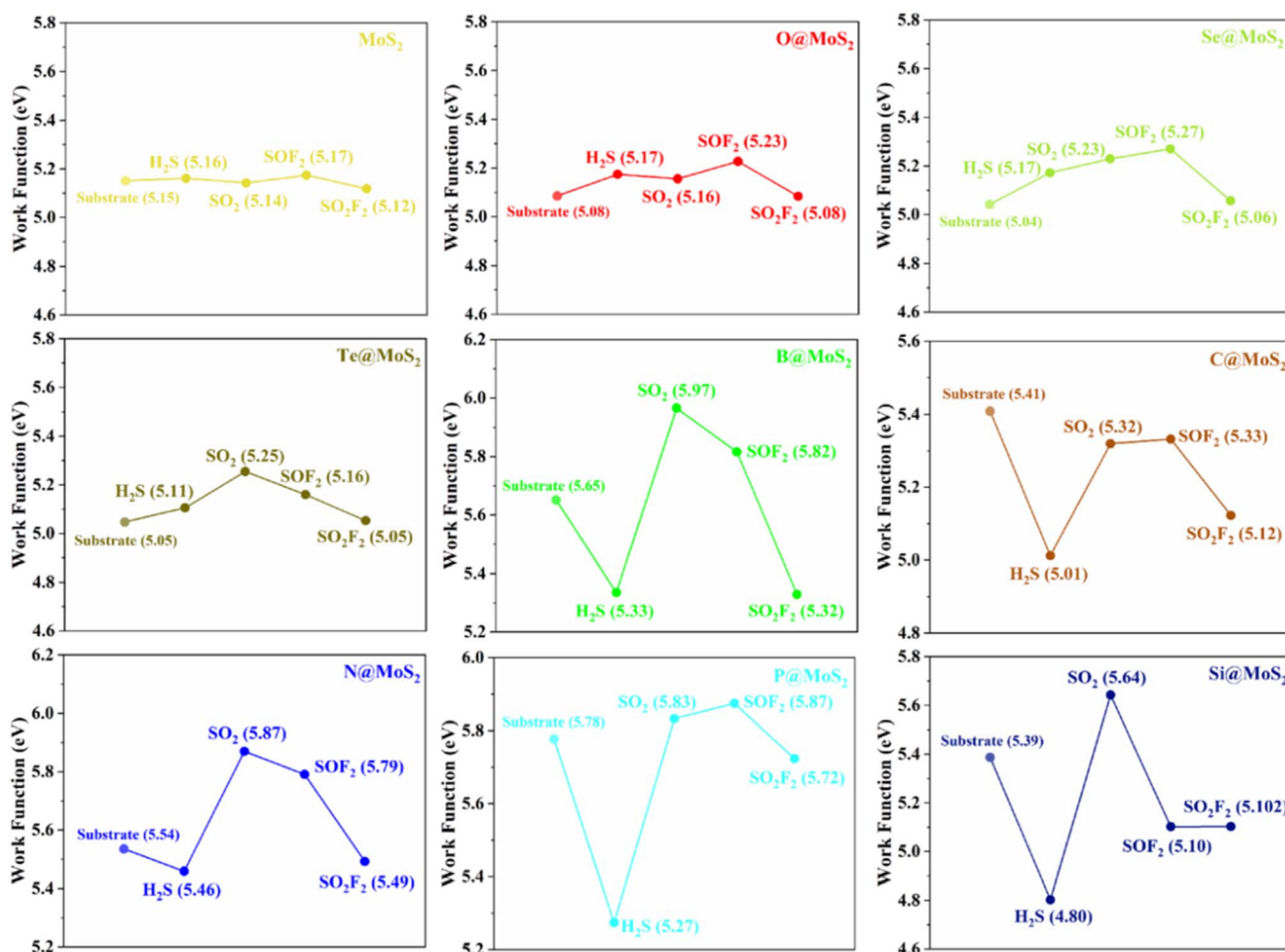


Fig. 6 Work function of four gases before and after adsorption on MoS₂, O@MoS₂, Se@MoS₂, Te@MoS₂, B@MoS₂, C@MoS₂, N@MoS₂, P@MoS₂, and Si@MoS₂ substrates, respectively.



accelerating the gas desorption process and improving the recycling of the B@MoS₂, C@MoS₂ and Si@MoS₂ substrates. Nevertheless, it is feasible to reduce the recovery time for the SOF₂/B@MoS₂, SO₂/C@MoS₂, SOF₂/C@MoS₂ and SO₂/C@MoS₂ adsorption systems by increasing the temperature. For example, at 398 K, the desorption times for the SOF₂/B@MoS₂ and SOF₂/C@MoS₂ systems are reduced to 2.23 and 5.13 seconds, respectively. Notably, the recovery times for the P@MoS₂ and Si@MoS₂ substrates are relatively short: at 298 K, the recovery times are 3.39 and 2.82 s for SO₂ and SO₂F₂ gases, respectively. This suggests that both the P@MoS₂ and Si@MoS₂ substrates can rapidly desorb SO₂ and SO₂F₂ at ambient temperature, indicating excellent recyclability.

3.4. Response capability

The work function is defined as the minimum energy required to move an electron from the surface of a material into a vacuum.⁷⁶ As a key parameter characterizing the surface electronic structure of sensing materials, its variation can quantitatively reflect the degree of charge transfer between gas

molecules and the material surface, thereby providing an important indication of the potential response capability of the sensing material. Thus, we systematically calculated the work functions (Φ) and the percentage change in work function ($\Delta\Phi\%$) of four gases before and after adsorption on pristine MoS₂ and NM@MoS₂ substrates. Φ and $\Delta\Phi\%$ can be calculated using eqn (4) and (5):

$$\Phi = V_{\text{Vacuum}} - V_{\text{Fermi}} \quad (4)$$

$$\Delta\Phi\% = (|\Phi_{\text{Unadsorbed}} - \Phi_{\text{adsorbed}}|/\Phi_{\text{Unadsorbed}}) \times 100\% \quad (5)$$

where V_{Vacuum} , V_{Fermi} , $\Phi_{\text{Unadsorbed}}$, and Φ_{adsorbed} represent the vacuum energy level, Fermi energy level, the work function of the substrate, and the work function for molecular adsorption on the substrate, respectively. The results are shown in Fig. 6 and 7.

Although the work function of the material increases slightly with the substitution of B, C, N, P and Si atoms, it remains lower than that of h-BN (5.986 eV) and Ti₃C₂O₂ MXene (5.97 eV).^{77,78} It is noteworthy that when the four gases adsorb onto the pristine

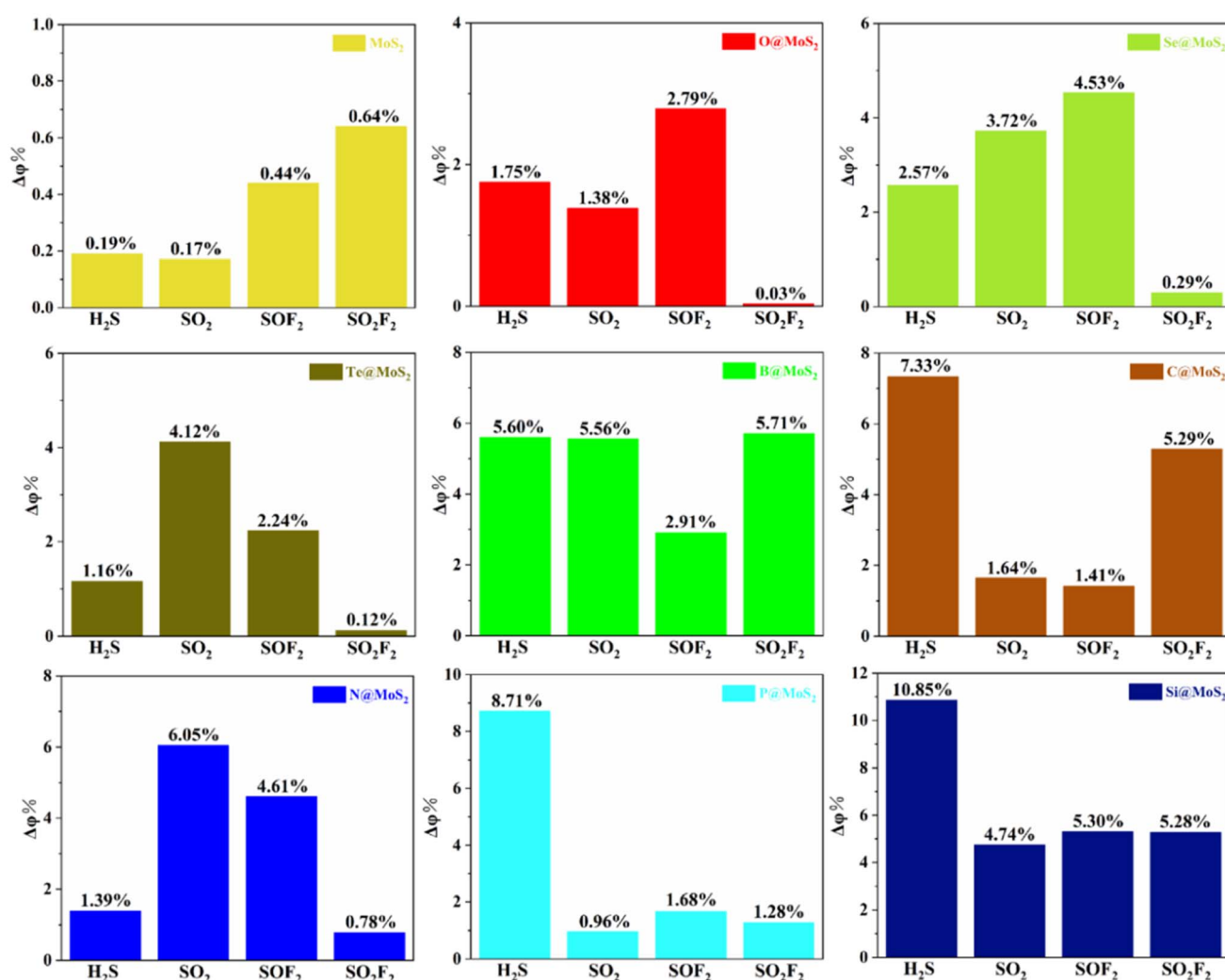


Fig. 7 The percentage change in work function of four gases after adsorption on MoS₂, O@MoS₂, Se@MoS₂, Te@MoS₂, B@MoS₂, C@MoS₂, N@MoS₂, P@MoS₂, and Si@MoS₂ substrates, respectively.

MoS_2 surface, $\Delta\Phi\%$ ranges from 0.17% to 0.64%, indicating that monolayer MoS_2 exhibits low response to these gases. Similar observations were made in the case of the SO_2F_2 -chalcogen substituted systems, where $\Delta\Phi\%$ ranged from 0.03% to 0.29%. The response of the other three adsorbed gases in the chalcogen substitution system increased slightly, with $\Delta\Phi\%$ ranging from 1.16% to 4.53%. In non-chalcogen-substituted systems, particularly in the cases of Si@MoS_2 and B@MoS_2 , the $\Delta\Phi\%$ range of was found to be 4.74% to 10.85% and 2.91% to 5.71%, respectively. This demonstrates that the substrate exhibits a high response to all four of these gases. While the C@MoS_2 , N@MoS_2 and P@MoS_2 substrates cannot maintain high response for all four gases simultaneously, they do significantly enhance the response of one or tow of these four gases. If it were possible, combining N@MoS_2 and C@MoS_2 materials achieves concurrent high-response of all four gases.

In summary, the theoretical analysis of work function variation and gas-solid adsorption interactions suggests that B@MoS_2 and Si@MoS_2 substrates both have high potential for responding to SF_6 decomposition gases. Therefore, they can be considered promising candidate sensing materials for all four target gases. Furthermore, combining N@MoS_2 and C@MoS_2 substrates enhances the theoretical response potential towards the four gases even further, suggesting a feasible strategy for optimising the sensing performance of MoS_2 -based materials.

However, the boundaries between theoretical predictions and practical sensing performance must be clarified, as must the limitations of the current computational model. This is necessary in order to contextualize the significance of these results. Although work function modulation indicates the potential sensing response, it differs from actual sensitivity, which depends on various factors, such as surface coverage, doping concentrations and humidity. The current model makes idealized assumptions (uniform doping, single-gas saturated adsorption and ignoring humidity), which deviate from reality. Future experimental work in this field should therefore consider controllable synthesis, testing in humid conditions, and optimizing the model with realistic parameters.

4. Conclusion

In the present study, DFT calculations were utilized to systematically explore the adsorption characteristics of NM@MoS_2 in relation to four SF_6 decomposition gases (H_2S , SO_2 , SOF_2 , SO_2F_2). The aim was to enhance the gas-detection efficacy of MoS_2 . The key findings are summarized below:

(1) According to the formation energy calculations for NM@MoS_2 , the results suggest that substitution at the S site is more feasible than substitution at the Mo site, as the former exhibits a lower (more negative) formation energy.

(2) Pristine MoS_2 shows weak physisorption for the target gases, with low adsorption energies (-0.21 to -0.33 eV), large adsorption distances (2.90 to 3.70 Å) and minimal charge transfer, which limits its sensing efficiency.

(3) The substitution systems involving chalcogen elements (O, Se and Te) retain the original surface characteristics of MoS_2 and have no significant impact on the adsorption behavior of

SF_6 decomposition products. In contrast, substitution systems involving non-chalcogen elements (B, C, N, P and Si) exhibit distinct adsorption properties, indicating that surface modification significantly alters gas adsorption behaviour.

(4) Recovery time analysis indicates that temperature control can optimize reusability. In particular, P@MoS_2 and Si@MoS_2 exhibit moderate recovery times for SO_2 and SO_2F_2 at ambient temperature, demonstrating their potential for repeated use in gas sensing.

(5) Work functional analysis confirms that NM atomic substitution significantly enhances the response capability of the intrinsic MoS_2 surface's response to SF_6 decomposition gas. The B@MoS_2 and Si@MoS_2 surfaces demonstrate a potential gas-sensing response to these gases.

Overall, non-metal doping is a viable strategy for enhancing the gas-sensing response of MoS_2 towards SF_6 decomposition products. This study provides valuable theoretical insights for designing high-sensitivity, reusable gas sensors for monitoring the safety of GIS operation.

Author contributions

Mamutjan Tursun: conceptualization, data curation, writing – original draft, Funding acquisition; Yifan Liu: data curation, formal analysis; Abulimiti Yumaier: data curation, formal analysis.

Conflicts of interest

There are no conflicts to declare.

Data availability

The authors confirm that the data supporting the findings of this study are available within the article and as its supplementary information (SI). Supplementary information: structure of NM atoms replacing Mo sites in monolayer MoS_2 ; formation energies of NM atoms substitution at Mo sites in monolayer MoS_2 ; comparison of adsorption energies for SF_6 -decomposition gases; references. See DOI: <https://doi.org/10.1039/d5ra08522e>.

Acknowledgements

We thank the financial support from the “Tianchi Talented young Doctors Program of Xinjiang Uygur Autonomous Region”, “Fundamental Research Grants for Universities in the Autonomous Region (Grant No. XJEDU2024P114)”, “Tianshan Innovation Team Plan of Xinjiang Uygur Autonomous Region (2023D14002)”, and the “Research Initiation Fund for High-level Talents at Kashi University (Grant No. GCC2023ZK-008)”.

References

- 1 A. Dong and M. Liu, A DFT study on the adsorption properties of $\text{Ti}_3\text{C}_2\text{O}_2$ MXene towards SF_6 decomposition gases, *Surf. Sci.*, 2023, **734**, 122317.



2 E. Mohammadi, Z. K. Horastani and A. K. Horestani, DFT Study of SO_2F_2 and SOF_2 Adsorption on (6,0) AlN Nanotube: Adsorbent and Gas Detector Toward SF_6 Decomposition Products, *IEEE Sens. J.*, 2025, **25**, 14646-14657.

3 H. Liu, F. Wang, K. Hu, T. Li, Y. Yan and J. Li, The Adsorption and Sensing Performances of Ir-modified MoS_2 Monolayer toward SF_6 Decomposition Products: A DFT Study, *Nanomaterials*, 2021, **11**, 100.

4 W. Zhou, Z. Li, L. Li, W. Zeng and Q. Zhou, Adsorption and detection of SF_6 decomposed toxic gases (H_2S , SO_2 , SOF_2 , SO_2F_2) on transition metal (Fe, Ru, Os) modified WTe_2 monolayer: A DFT investigation, *J. Environ. Chem. Eng.*, 2025, **13**, 115545.

5 Z. Shi, Y. Zhang, W. Zeng and Q. Zhou, A DFT study on adsorption of SF_6 decomposition gases (H_2S , SO_2 , SO_2F_2 and SOF_2) on Sc- MoTe_2 monolayer, *Sens. Actuators. A Phys.*, 2023, **360**, 114548.

6 S.-Y. Xia, L.-Q. Tao, T. Jiang, H. Sun and J. Li, Rh-doped h-BN monolayer as a high sensitivity SF_6 decomposed gases sensor: A DFT study, *Appl. Surf. Sci.*, 2021, **536**, 147965.

7 M. Wang, J. Cao, P. Jia, Y. Zhang, J. Liu, M. Xu and D. Chen, Research on high-performance materials for adsorption and monitoring of SF_6 and its decomposed gases: First principle DFT calculations, *Mater. Chem. Phys.*, 2025, **335**, 130533.

8 Y. Yang, L. Huang, W. Zeng and Q. Zhou, Metal clusters (Pt_3 and Pd_3) modified InSe monolayer: An adsorbent and gas sensor for SF_6 decomposition gases (SO_2 , H_2S , SOF_2 , SO_2F_2) based on density functional theory, *J. Environ. Chem. Eng.*, 2025, **13**, 117095.

9 A. K. Pandey and A. K. Mishra, Angle-dependent growth of 2D MoS_2 monolayer, bilayer by chemical vapor deposition method, *Phys. Scr.*, 2025, **100**, 075938.

10 P. Prajapat, A. A. Chaudhary, A. Yadav, V. Kandwal, P. Vashishtha, M. A. M. Ali, S. Walia and G. Gupta, Enhancement in hazardous gas detection capabilities of MoS_2 monolayer-based devices through defect engineering and photonic activation, *Sci. Rep.*, 2025, **15**, 39174.

11 J. He, T. Yao, Y. Xiong and F. Xie, High gas-sensing performance of SF_6 decomposition gases on $\text{PdSe}_2/\text{MoS}_2$ heterojunction: A DFT study, *Comput. Theor. Chem.*, 2025, **1251**, 115330.

12 C. Xue, L. Lin, K. Xie, Z. Zhang and P. Wang, Adsorption of toxic gases by Janus MoSeTe monolayers doped with transition metals and surface defects: A first-principles study, *Colloids Surf. A*, 2024, **694**, 134131.

13 G. Sanyal, A. Vaidyanathan, C. S. Rout and B. Chakraborty, Recent developments in two-dimensional layered tungsten dichalcogenides based materials for gas sensing applications, *Mater. Today Commun.*, 2021, **28**, 102717.

14 W. Zheng, X. Liu, J. Xie, G. Lu and J. Zhang, Emerging van der Waals junctions based on TMDs materials for advanced gas sensors, *Coord. Chem. Rev.*, 2021, **447**, 214151.

15 F. Li, H. Wu and H. Cui, Favorable adsorption and sensing properties of the HfS_2 monolayer upon H_2S and SOF_2 gases by Pt-doping: A first-principles study, *Comput. Theor. Chem.*, 2025, **1244**, 115031.

16 S. Jiang, F. Li and H. Cui, First-Principles Insight Into Adsorption Characteristics of Ir-Embedded HfS_2 Monolayers for Gas-Sensing of H_2S , SOF_2 , and SO_2F_2 , *ChemistrySelect*, 2025, **10**, e01393.

17 L. Wang, D. Xu, L. Jiang, J. Gao, Z. Tang, Y. Xu, X. Chen and H. Zhang, Transition Metal Dichalcogenides for Sensing and Oncotherapy: Status, Challenges, and Perspective, *Adv. Funct. Mater.*, 2021, **31**, 2004408.

18 S. A. Kadam, Advancements in monolayer TMD-based gas sensors: Synthesis, mechanisms, electronic structure engineering, and flexible wearable sensors for real-world applications and future prospects, *Chem. Eng. J.*, 2025, **517**, 164223.

19 F. Jiang, W.-S. Zhao and J. Zhang, Mini-review: Recent progress in the development of MoSe_2 based chemical sensors and biosensors, *Microelectron. Eng.*, 2020, **225**, 111279.

20 R. K. Mishra, H. J. Choi, J. W. Ryu, G. J. Choi, V. Kumar, P. Kumar, J. Singh, S. Kumar and J. S. Gwag, Recent progress in gas sensing based on 2D SnS_2 and its heterostructure platforms: A review, *Sens. Actuators. A Phys.*, 2024, **365**, 114860.

21 X. Wang and J. Wang, Effects of Pt and Au adsorption on the gas sensing performance of SnS_2 monolayers: A DFT study, *Mater. Sci. Semicond. Process.*, 2021, **121**, 105416.

22 S. Kumar, A. Mirzaei, A. Kumar, M. Hoon Lee, Z. Ghahremani, T.-U. Kim, J.-Y. Kim, M. Kwoka, M. Kumar, S. Sub Kim and H. Woo Kim, Nanoparticles anchored strategy to develop 2D MoS_2 and MoSe_2 based room temperature chemiresistive gas sensors, *Coord. Chem. Rev.*, 2024, **503**, 215657.

23 I. Shahbaz, M. Tahir, L. Li and Y. Song, Advancements in 2D transition metal dichalcogenides (TMDs) inks for printed optoelectronics: A comprehensive review, *Mater. Today*, 2024, **77**, 142-184.

24 S. Susarla, A. Kutana, J. A. Hachtel, V. Kochat, A. Apte, R. Vajtai, J. C. Idrobo, B. I. Yakobson, C. S. Tiwary and P. M. Ajayan, 2D Materials: Quaternary 2D Transition Metal Dichalcogenides (TMDs) with Tunable Bandgap, *Adv. Mater.*, 2017, **29**, 1702457.

25 H. Schmidt, F. Giustiniano and G. Eda, Electronic transport properties of transition metal dichalcogenide field-effect devices: surface and interface effects, *Chem. Soc. Rev.*, 2015, **44**, 7715-7736.

26 M. Schleicher and M. Fyta, Lateral MoS_2 Heterostructure for Sensing Small Gas Molecules, *ACS Appl. Electron. Mater.*, 2020, **2**, 74-83.

27 R. Du and W. Wu, Adsorption of gas molecule on Rh, Ru doped monolayer MoS_2 for gas sensing applications: A DFT study, *Chem. Phys. Lett.*, 2022, **789**, 139300.

28 D. J. Late, Y.-K. Huang, B. Liu, J. Acharya, S. N. Shirodkar, J. Luo, A. Yan, D. Charles, U. V. Waghmare, V. P. Dravid and C. N. R. Rao, Sensing Behavior of Atomically Thin-Layered MoS_2 Transistors, *ACS Nano*, 2013, **7**, 4879-4891.

29 T. Pham, G. Li, E. Bekyarova, M. E. Itkis and A. Mulchandani, MoS_2 -Based Optoelectronic Gas Sensor with Sub-parts-per-



billion Limit of NO₂ Gas Detection, *ACS Nano*, 2019, **13**, 3196–3205.

30 J. Cha, K.-A. Min, D. Sung and S. Hong, Ab initio study of adsorption behaviors of molecular adsorbates on the surface and at the edge of MoS₂, *Curr. Appl. Phys.*, 2018, **18**, 1013–1019.

31 J. Zhu, H. Zhang, Y. Tong, L. Zhao, Y. Zhang, Y. Qiu and X. Lin, First-principles investigations of metal (V, Nb, Ta)-doped monolayer MoS₂: Structural stability, electronic properties and adsorption of gas molecules, *Appl. Surf. Sci.*, 2017, **419**, 522–530.

32 M. Yin, K. Wang, C. Gao, R. Yang, Y. Huang and L. Yu, Synthesis and insights into the gas sensing mechanisms of N-doped MoS₂ hierarchical structures with superior gas sensing properties at room temperature, *Mater. Res. Bull.*, 2024, **179**, 112943.

33 R. Zhang, D. Fu, J. Ni, C. Sun and S. Song, Adsorption for SO₂ gas molecules on B, N, P and Al doped MoS₂: The DFT study, *Chem. Phys. Lett.*, 2019, **715**, 273–277.

34 N. N. Viet, L. V. Thong, T. K. Dang, P. H. Phuoc, N. H. Chien, C. M. Hung, N. D. Hoa, N. Van Duy, N. Van Toan, N. T. Son and N. Van Hieu, MoS₂ nanosheets-decorated SnO₂ nanofibers for enhanced SO₂ gas sensing performance and classification of CO, NH₃ and H₂ gases, *Anal. Chim. Acta*, 2021, **1167**, 338576.

35 W. Guo, K. Chen, S. Wang, H. Zhang and D. Wu, Dual functionalized flower-like MoS₂ nanospheres with Pd and g-C₃N₄ for triethylamine gas sensing performance, *Sens. Actuators. B Chem.*, 2025, **433**, 137490.

36 Y. Gui, J. Shi, P. Yang, T. Li, C. Tang and L. Xu, Platinum modified MoS₂ monolayer for adsorption and gas sensing of SF₆ decomposition products: a DFT study, *High Voltage*, 2020, **5**, 454–462.

37 Y. Fan, J. Zhang, Y. Qiu, J. Zhu, Y. Zhang and G. Hu, A DFT study of transition metal (Fe, Co, Ni, Cu, Ag, Au, Rh, Pd, Pt and Ir)-embedded monolayer MoS₂ for gas adsorption, *Comput. Mater. Sci.*, 2017, **138**, 255–266.

38 H. Luo, Y. Cao, J. Zhou, J. Feng, J. Cao and H. Guo, Adsorption of NO₂, NH₃ on monolayer MoS₂ doped with Al, Si, and P: A first-principles study, *Chem. Phys. Lett.*, 2016, **643**, 27–33.

39 A. V. Agrawal, N. Kumar and M. Kumar, Strategy and Future Prospects to Develop Room-Temperature-Recoverable NO₂ Gas Sensor Based on Two-Dimensional Molybdenum Disulfide, *Nanomicro. Lett.*, 2021, **13**, 38.

40 Z. Cui, X. Zhang, Y. Li, D. Chen, Y. Li and H. Xiao, Theoretical study of SF₆ decomposition on the MoS₂ monolayer doped with Ag, Ni, Au, Pt: a first-principles study, *Adsorption*, 2019, **25**, 225–233.

41 B. Li, Q. Zhou, R. Peng, Y. Liao and W. Zeng, Adsorption of SF₆ decomposition gases (H₂S, SO₂, SOF₂ and SO₂F₂) on Sc-doped MoS₂ surface: A DFT study, *Appl. Surf. Sci.*, 2021, **549**, 149271.

42 M. J. Szary, MoS₂ doping for enhanced H₂S detection, *Appl. Surf. Sci.*, 2021, **547**, 149026.

43 E. Piosik and M. J. Szary, Development of MoS₂ doping strategy for enhanced SO₂ detection at room temperature, *Appl. Surf. Sci.*, 2023, **638**, 158013.

44 D. Ma, Q. Wang, T. Li, C. He, B. Ma, Y. Tang, Z. Lu and Z. Yang, Repairing sulfur vacancies in the MoS₂ monolayer by using CO, NO and NO₂ molecules, *J. Mater. Chem. C Mater.*, 2016, **4**, 7093–7101.

45 H. Huang, X. Feng, C. Du and W. Song, High-quality phosphorus-doped MoS₂ ultrathin nanosheets with amenable ORR catalytic activity, *Chem. Commun.*, 2015, **51**, 7903–7906.

46 J. Xie, J. Zhang, S. Li, F. Grote, X. Zhang, H. Zhang, R. Wang, Y. Lei, B. Pan and Y. Xie, Controllable Disorder Engineering in Oxygen-Incorporated MoS₂ Ultrathin Nanosheets for Efficient Hydrogen Evolution, *J. Am. Chem. Soc.*, 2013, **135**, 17881–17888.

47 H. Huang, X. Feng, C. Du, S. Wu and W. Song, Incorporated oxygen in MoS₂ ultrathin nanosheets for efficient ORR catalysis, *J. Mater. Chem. A Mater.*, 2015, **3**, 16050–16056.

48 M. Zhu, Y. Zhang, S. Xu, X. Yan, Y. Song, M. Wang, Y. Dong and J. Zhang, Enhanced lithium-sulfur battery electrochemistry via Se-doped MoS₂/rGO ultrathin sheets as sulfur hosts, *Appl. Surf. Sci.*, 2025, **682**, 161718.

49 Y. Luo, K. Chen, P. Shen, X. Li, X. Li, Y. Li and K. Chu, B-doped MoS₂ for nitrate electroreduction to ammonia, *J. Colloid Interface Sci.*, 2023, **629**, 950–957.

50 X. Chen, S. Lu, Y. Wei, M. Sun, X. Wang, M. Ma and J. Tian, Basal Plane-Activated Boron-Doped MoS₂ Nanosheets for Efficient Electrochemical Ammonia Synthesis, *ChemSusChem*, 2023, **16**, e202202265.

51 S. Chen, D. Fang, Z. Zhou, Z. Zhao, Y. Yang, Z. Dai and J. Shi, B-doped MoS₂/MoO₂ heterostructure catalyst for the electrocatalytic reduction of N₂ to NH₃, *Catal. Lett.*, 2024, **154**, 4055–4064.

52 G. Kresse and J. Furthmüller, Efficiency of ab-initio total energy calculations for metals and semiconductors using a plane-wave basis set, *Comput. Mater. Sci.*, 1996, **6**, 15–50.

53 J. P. Perdew, K. Burke and M. Ernzerhof, Generalized Gradient Approximation Made Simple, *Phys. Rev. Lett.*, 1996, **77**, 3865–3868.

54 P. E. Blöchl, Projector augmented-wave method, *Phys. Rev. B: Condens. Matter Mater. Phys.*, 1994, **50**, 17953–17979.

55 L. Goerigk, A Comprehensive Overview of the DFT-D3 London-Dispersion Correction, in: *Non-Covalent Interactions in Quantum Chemistry and Physics*, Elsevier, 2017, pp. 195–219.

56 T. Lu and F. Chen, Revealing the nature of intermolecular interaction and configurational preference of the nonpolar molecular dimers (H₂)₂, (N₂)₂, and (H₂)(N₂), *J. Mol. Model.*, 2013, **19**, 5387–5395.

57 J. B. A. Davis, F. Baletto and R. L. Johnston, The Effect of Dispersion Correction on the Adsorption of CO on Metallic Nanoparticles, *J. Phys. Chem. A*, 2015, **119**, 9703–9709.

58 P. P. Mkhonto, X. Zhang, L. Lu, W. Xiong, Y. Zhu, L. Han and P. E. Ngoepe, Design, synthesis and investigating the interaction of novel s-triazine collector with pyrite surface:



A DFT-D3+U and experimental studies, *Surf. Interfaces*, 2023, **38**, 102820.

59 K. Boezar, A. Reisi-Vanani and M. Dehkhodaei, Modification of graphenylene nanostructure with transition metals (Fe, Sc and Ti) to promote hydrogen storage ability: A DFT-D3 study, *Int. J. Hydrogen Energy*, 2021, **46**, 38370–38380.

60 D. J. Chadi and M. L. Cohen, Special Points in the Brillouin Zone, *Phys. Rev. B: Condens. Matter Mater. Phys.*, 1973, **8**, 5747–5753.

61 Y. Fu, X. Feng, M.-F. Yan, K. Wang and S. Wang, First principle study on electronic structure and optical phonon properties of 2H-MoS₂, *Phys. B Condens. Matter*, 2013, **426**, 103–107.

62 Y. Zhao, Y. Chen, P. Ou and J. Song, Basal Plane Activation via Grain Boundaries in Monolayer MoS₂ for Carbon Dioxide Reduction, *ACS Catal.*, 2023, **13**, 12941–12951.

63 W. Xiao, P. Liu, J. Zhang, W. Song, Y. P. Feng, D. Gao and J. Ding, Dual-Functional N Dopants in Edges and Basal Plane of MoS₂ Nanosheets Toward Efficient and Durable Hydrogen Evolution, *Adv. Energy Mater.*, 2017, **7**, DOI: [10.1002/aenm.201602086](https://doi.org/10.1002/aenm.201602086).

64 P. Tao, J. He, T. Shen, Y. Hao, J. Yan, Z. Huang, X. Xu, M. Li and Y. Chen, Nitrogen-Doped MoS₂ Foam for Fast Sodium Ion Storage, *Adv. Mater. Interfaces*, 2019, **6**, 1900460.

65 D. Yuan, C. Guo, Y. Ning, X. Fu, X. Li, X. Xu, C. Wang, Y. Kou and J. Cui, N-Doped Modified MoS₂ for Piezoelectric-Photocatalytic Removal of Tetracycline: Simultaneous Improvement of Photocatalytic and Piezoelectric Properties, *Water*, 2025, **17**, 1296.

66 L. Song, M. Song, Z. Lu, G. Yu, Z. Liang, W. Hou, Q. Liao and Y. Song, Recent Advances of Preparation and Application of Two-Dimension van der Waals Heterostructure, *Coatings*, 2022, **12**, 1152.

67 Y. Gui, J. Chen, W. Wang, Y. Zhu, C. Tang and L. Xu, Adsorption mechanism of hydrogen sulfide and sulfur dioxide on Au-MoS₂ monolayer, *Superlattices Microstruct.*, 2019, **135**, 106280.

68 H. Wei, Y. Gui, J. Kang, W. Wang and C. Tang, A DFT Study on the Adsorption of H₂S and SO₂ on Ni Doped MoS₂ Monolayer, *Nanomaterials*, 2018, **8**, 646.

69 D. Chen, X. Zhang, J. Tang, Z. Cui, H. Cui and S. Pi, Theoretical Study of Monolayer PtSe₂ as Outstanding Gas Sensor to Detect SF₆ Decompositions, *IEEE Electr. Device L.*, 2018, **39**, 1405–1408.

70 T.-Y. Sang, T. Li, Y. Yang, Y. Song, H. Tian, R. Song, C. Wang, X. Hu, Z. Yang, Y. Lu and W. Chen, Pd, Rh-decorated Se-vacancy MoSe₂ monolayer: A promising candidate for sensing and detecting SO₂F₂, SOF₂, H₂S and SO₂, *Surf. Interfaces*, 2022, **33**, 102269.

71 X. Zhou, J. Bai, H. Cui, T. Tian, Y. Luo and L. Tian, Outstanding sensing property of Cu-substituted MoTe₂ monolayer upon SF₆ decomposed species from first-principles calculations, *Comput. Theor. Chem.*, 2023, **1228**, 114273.

72 Z. Xu, H. Cui and G. Zhang, Pd-Decorated WTe₂ Monolayer as a Favorable Sensing Material toward SF₆ Decomposed Species: A DFT Study, *ACS Omega*, 2023, **8**, 4244–4250.

73 Z. Wang, M. Wang and X. Hu, Adsorption and sensing performances of greenhouse gases (CO₂, CH₄, N₂O, and SF₆) on pristine and Pd-doped GeSe monolayer: A DFT study, *Sens. Actuators. A Phys.*, 2024, **370**, 115222.

74 Z. Wang, T. Xia and X. Hu, Metal Oxide (Ag₂O, ZnO)-Doped MoSe₂ Monolayer as a Highly Sensitive Gas Sensor for Greenhouse Gases (CO₂, CH₄, N₂O, SF₆) Detection, *ACS Appl. Nano Mater.*, 2024, **7**, 20994–21004.

75 M. Mohammadi and E. Pakizeh, SiB Monolayers-Based Gas Sensor: Work Function and Conductometric Type Gas Sensors, *Adv. Theory. Simul.*, 2025, **8**, 2401127.

76 P. Hurdax, M. Hollerer, C. S. Kern, P. Puschnig, M. Sterrer and M. G. Ramsey, Integer Charge Transfer Model–PTCDA on MgO(001)/Ag(001) Probing the Transition from Single to Double Integer Charge Transfer, *J. Phys. Chem. C*, 2025, **129**, 1553–1561.

77 B. Yu, H. Ren and X. Piao, Towards Adsorptive Enrichment of Flavonoids from Honey Using h-BN Monolayer, *ChemPhysChem*, 2022, **23**, e202100828.

78 R. Li, W. Sun, C. Zhan, P. R. C. Kent and D. Jiang, Interfacial and electronic properties of heterostructures of MXene and graphene, *Phys. Rev. B: Condens. Matter Mater. Phys.*, 2019, **99**, 085429.

